Achieving the Scaling Limit for Nonequilibrium Green Functions Simulations

Niclas Schlünzen, Jan-Philip Joost, and Michael Bonitz
Institut für Theoretische Physik und Astrophysik, Christian-Albrechts-Universität zu Kiel, D-24098 Kiel, Germany

(Received 26 September 2019; accepted 24 December 2019; published 19 February 2020)

The dynamics of strongly correlated fermions following an external excitation reveals extremely rich collective quantum effects. Examples are fermionic atoms in optical lattices, electrons in correlated materials, and dense quantum plasmas. Presently, the only quantum-dynamics approach that rigorously describes these processes in two and three dimensions is the nonequilibrium Green functions (NEGF) method. However, NEGF simulations are computationally expensive due to their T^3 scaling with the simulation duration T. Recently, T^2 scaling was achieved with the generalized Kadanoff-Baym ansatz (GKBA), for second-order Born (SOA) selfenergies, which has substantially extended the scope of NEGF simulations. Here we demonstrate that GKBA-NEGF simulations can be performed with order T^1 scaling, both for SOA and GW selfenergies, and point out the remarkable capabilities of this approach.

DOI: 10.1103/PhysRevLett.124.076601

Strongly correlated fermion systems are attracting increasing interest in many fields including dense plasmas [1,2], warm dense matter [3,4], strongly correlated materials [5,6], ultracold atoms [7,8], and atoms and molecules in strong radiation fields [9,10]. Of particular relevance are the relaxation phenomena that occur following an external excitation such as a rapid change ("quench") of the confinement or the interaction strength, the impact of charged particles [11,12], or the photoionization of atoms by lasers or free-electron lasers [13,14]. Many theoretical approaches to the dynamics of strongly correlated fermions are limited either to one-dimensional systems (density-matrix renormalization-group simulations, DMRG) or short times (quantum Monte Carlo). The first quantum simulations of the expansion of correlated fermions in two and three dimensions were recently achieved using nonequilibrium Green functions (NEGF) [8] and exhibited very good agreement with experiments. The high accuracy of NEGF simulations was also demonstrated by comparison to DMRG [15]. However, these NEGF simulations are hampered by an unfavorable scaling with the simulation duration according to T^3 resulting from the two-time structure of the NEGF and the memory effects in the collision integral (see below).

This behavior can be relieved by applying the generalized Kadanoff-Baym ansatz (GKBA) [16,17], which reduces the dynamics of the NEGF $G(t,t')$ to propagation along the time diagonal $t = t'$. It could be demonstrated that, indeed, the expected improvement of the scaling, $N_t^3 \to N_t^2$ (in the following we will use the number of discretization time steps $N_t = T/\Delta t$), can be achieved in practice for the selfenergy in the second-order Born approximation (SOA) [18,19] where initial correlation effects can be treated even more efficiently [20,21]. It could further be shown that this approximation, in many cases, does not lead to a loss of accuracy [10,15,22]. For these reasons, NEGF simulations using the GKBA with Hartree-Fock propagators (HF-GKBA) [cf. Eqs. (6) and (7) below] have become a powerful tool for studying the quantum dynamics in many fields, including optically excited semiconductors [23–25], excitonic insulators [26], quantum transport and molecular junctions [27,28], laser-excited plasmas [29,30] and atoms [10,13], strongly correlated electrons [22], and fermionic atoms in optical lattices [15,31]. In recent years, significant effort was devoted to improve the GKBA, see, e.g., Refs. [17,20–22,27,32–34]. Nevertheless, the quadratic scaling with N_t still makes the approach much less efficient than competing methods that scale linearly with N_t, such as molecular dynamics, fluid theory, time-dependent density-functional theory within the adiabatic approximation, or Boltzmann-type (Markovian) kinetic equations.

In this Letter we demonstrate that the same linear scaling with N_t, which is the ultimate limit in time-dependent simulations, can be achieved for NEGF simulations within the HF-GKBA. This allows for unprecedented long simulations as well as for high-quality energy spectra that are computed via Fourier transformation of time-dependent quantities, see, e.g., Refs. [35–37]. We demonstrate this efficiency gain, compared to the original HF-GKBA, for finite Hubbard clusters and predict an even stronger gain for a basis in which the Green function and selfenergy are diagonal, such as for spatially homogeneous systems. Moreover, our approach allows one to compute additional quantities that are not directly accessible in standard NEGF schemes, such as the time-dependent pair-distribution function, the static and dynamic structure factor, and various correlation functions. Finally, we prove that linear scaling can be achieved also for more advanced

selfenergies, such as GW, where all existing schemes scale as N_t^3.

Theory.—We consider a general many-particle system with the Hamiltonian

$$H(t) = \sum_{ij} h_{ij}(t)\hat{c}_i^\dagger \hat{c}_j + \frac{1}{2}\sum_{ijkl} w_{ijkl}\hat{c}_i^\dagger \hat{c}_j^\dagger \hat{c}_l \hat{c}_k, \qquad (1)$$

containing a single-particle contribution $\hat{h}$ and a pair interaction $\hat{w}$. The matrix elements are computed with an orthonormal system of single-particle orbitals $|i\rangle$. The creation ($\hat{c}_i^\dagger$) and annihilation ($\hat{c}_i$) operators of particles in state $|i\rangle$ define the one-body nonequilibrium Green functions (correlation functions; here and below "$\pm$" refers to bosons and fermions) $G_{ij}^<(t,t') = \pm(i/\hbar)\langle \hat{c}_j^\dagger(t')\hat{c}_i(t)\rangle$ and $G_{ij}^>(t,t') = (i/\hbar)\langle \hat{c}_i(t)\hat{c}_j^\dagger(t')\rangle$, where the averaging is performed with the correlated unperturbed density operator of the system. The response of the system (1) to an external excitation is described by the Keldysh-Kadanoff-Baym equations (KBE) on the time diagonal [16,19] where the Green function reduces to the single-particle density matrix, $\pm i\hbar G_{ij}^<(t,t) = n_{ij}(t)$,

$$\frac{\partial n_{ij}(t)}{\partial t} - \frac{1}{i\hbar}\sum_k [h_{ik}^{\mathrm{HF}}(t), n_{kj}(t)] = \pm[I + I^\dagger]_{ij}(t), \quad (2)$$

with a mean-field Hamiltonian h^{HF}. Here I is the collision integral that takes into account interaction effects beyond Hartree-Fock, including scattering and dissipation, which we will treat in leading order, i.e., within the SOA [19,38]:

$$I_{ij}(t) = (i\hbar)^2 \sum_{mnp} w_{imnp}(t) \sum_{kqrs} \int_{t_0}^{t} d\bar{t}\, w_{qrsk}^{\pm}(\bar{t}) \times [G_{nq}^>(t,\bar{t})G_{pr}^>(t,\bar{t})G_{sm}^<(\bar{t},t)G_{kj}^<(\bar{t},t) - (> \leftrightarrow <)], \qquad (3)$$

where we defined $w_{qrsj}^{\pm} \equiv w_{qrsj} \pm w_{qrjs} = \pm w_{qrjs}^{\pm}$. Clearly, the computational effort to solve Eqs. (2) and (3) scales with the number of time steps as N_t^2.

We now demonstrate that, in the HF-GKBA approximation, Eqs. (2) and (3) can be reformulated such that the effort is reduced to N_t^1 scaling. First, we introduce an auxiliary four-index function $\mathcal{G}$,

$$I_{ij}(t) = \pm i\hbar \sum_{mnp} w_{imnp}(t)\mathcal{G}_{npjm}(t), \qquad (4)$$

$$\mathcal{G}_{npjm}(t) = i\hbar \sum_{kqrs} \int_{t_0}^{t} d\bar{t}\, w_{qrsk}^{\pm}(\bar{t}) \times [G_{nq}^>(t,\bar{t})G_{pr}^>(t,\bar{t})G_{sj}^<(\bar{t},t)G_{km}^<(\bar{t},t) - (> \leftrightarrow <)], \qquad (5)$$

where the replacement $k \leftrightarrow s$ is used to match Eq. (3). Comparing Eq. (4) with the first equation of the Martin-Schwinger hierarchy for the many-particle Green functions [39] reveals that $\mathcal{G}(t)$ is nothing but the time-diagonal element of the two-particle Green function, and Eq. (5) is its explicit form in the second-Born approximation [40]. Next, we introduce the GKBA [16,19] (summation over k is implied)

$$G_{ij}^{\gtrless}(t,t') = \pm G_{ik}^R(t,t')n_{kj}^{\gtrless}(t') \mp n_{ik}^{\gtrless}(t)G_{kj}^A(t,t'), \qquad (6)$$

$$G^{R/A}(t,t') = \Theta[+/-(t-t')]\{G^{\gtrless}(t,t') - G^{\lessgtr}(t,t')\},$$
$$n_{ij}^<(t) = n_{ij}(t), \qquad n_{ij}^>(t) = n_{ij}(t) - \delta_{ij}, \qquad (7)$$

with Hartree-Fock propagators (HF-GKBA), $G^{R/A} \to G^{R/A,\mathrm{HF}}$ and apply it to each Green function in Eq. (5):

$$\mathcal{G}_{npjm}^{\mathrm{GKBA}}(t) = i\hbar \sum_{abcdkqrs} \int_{t_0}^{t} d\bar{t}\, w_{qrsk}^{\pm}(\bar{t}) \times \mathcal{U}_{npab}^{(2)}(t,\bar{t})\Phi_{qrcd}^{absk}(\bar{t})\mathcal{U}_{cdjm}^{(2)}(\bar{t},t). \qquad (8)$$

Here we introduced the abbreviations

$$\Phi_{qrcd}^{absk}(t) = \Phi_{qrcd}^{absk>}(t) - \Phi_{qrcd}^{absk<}(t),$$
$$\Phi_{qrcd}^{absk\gtrless}(t) = n_{qa}^{\gtrless}(t)n_{rb}^{\gtrless}(t)n_{cs}^{\lessgtr}(t)n_{dk}^{\lessgtr}(t), \qquad (9)$$

and the two-particle time-evolution operator $\mathcal{U}^{(2)}$ is given in the Supplemental Material [41].

Finally, we remove the time integral in Eq. (8) by differentiating with respect to time which yields

$$i\hbar\frac{d}{dt}\mathcal{G}_{npjm}^{\mathrm{GKBA}}(t) - [h^{(2)\mathrm{HF}}, \mathcal{G}^{\mathrm{GKBA}}]_{npjm}(t) = \frac{1}{(i\hbar)^2}\sum_{kqrs} w_{qrsk}^{\pm}(t)\Phi_{qrjm}^{npsk}(t), \qquad (10)$$

where $h_{ijkl}^{(2)\mathrm{HF}}(t) = \delta_{jl}h_{ik}^{\mathrm{HF}}(t) + \delta_{ik}h_{jl}^{\mathrm{HF}}(t)$. With this we have shown that NEGF theory within the HF-GKBA can be brought to a memory-less form (10) which, indeed, changes the scaling from quadratic to linear with N_t. This was achieved by introducing the two-particle Green function on the time diagonal $\mathcal{G}$ and by solving coupled time-local equations for $G(t,t)$ and $\mathcal{G}(t)$. We, therefore, will refer to this as the "G1–G2" scheme. In fact, the one-to-one correspondence of NEGF theory within the HF-GKBA to time-local equations has been observed before [18,42]. In Ref. [42] it was also shown how to include arbitrary initial correlations, by supplementing Eq. (10) with an initial value, $\mathcal{G}^{\mathrm{GKBA}}(t_0) = \mathcal{G}_0$. In Eq. (8) this gives rise to an additional homogeneous solution that leads to an additional collision integral in the time-diagonal KBE (2), in agreement with recent results [20,21].

TABLE I. Scaling of the CPU time with the number of time steps N_t and basis dimension N_b of the traditional non-Markovian HF-GKBA and the present time-local scheme (G1–G2), for three relevant basis sets, for SOA and *GW* selfenergies.

Basis and pair potential	SOA		*GW*	
	Old	G1–G2	Old	G1–G2
General: w_{ijkl}	$\mathcal{O}(N_b^5 N_t^2)$	$\mathcal{O}(N_b^5 N_t^1)$	$\mathcal{O}(N_b^6 N_t^3)$	$\mathcal{O}(N_b^6 N_t^1)$
Hubbard: U	$\mathcal{O}(N_b^3 N_t^2)$	$\mathcal{O}(N_b^5 N_t^1)$	$\mathcal{O}(N_b^3 N_t^3)$	$\mathcal{O}(N_b^5 N_t^1)$
Jellium: $v_{\lvert\boldsymbol{q}\rvert}$	$\mathcal{O}(N_b^3 N_t^2)$	$\mathcal{O}(N_b^3 N_t^1)$	$\mathcal{O}(N_b^3 N_t^3)$	$\mathcal{O}(N_b^3 N_t^1)$

In the following we analyze the G1–G2 scheme more in detail. One readily confirms that the CPU time required to solve Eq. (10), for a general basis of dimension N_b, scales as $\mathcal{O}(N_b^5 N_t^1)$ [43]. In contrast, the original HF-GKBA scales as $\mathcal{O}(N_b^5 N_t^2)$ and, thus a dramatic speedup is expected, for any N_b [45]. At the same time, for many practical applications optimized basis sets are being used for which the scaling of both schemes has to be established separately. We, therefore, consider below two representative examples—the *Hubbard* basis and the uniform electron gas. The scaling for all three cases is summarized in Table I.

Hubbard basis.—The (Fermi-)Hubbard model is a key system in the theory of strongly correlated electrons in solids, see, e.g., Refs. [46,47], and it is being directly realized with fermionic atoms in optical lattices, see, e.g., Refs. [7,48,49]. It is defined by the Hubbard Hamiltonian

$$\hat{H}(t) = -J\sum_{\langle i,j\rangle}\sum_{\alpha}\hat{c}_{i\alpha}^{\dagger}\hat{c}_{j\alpha} + U(t)\sum_{i}\hat{n}_i^{\uparrow}\hat{n}_i^{\downarrow}, \qquad (11)$$

which includes hopping processes between nearest-neighbor sites $\langle i,j\rangle$ with amplitude J and an on-site interaction U, and α labels the spin projection. The integral (4) reads, $I_{ij}^{\uparrow(\downarrow)}(t) = -i\hbar U(t)\mathcal{G}_{iiji}^{\uparrow(\downarrow)}(t)$, and the equation of motion (10) for $\mathcal{G}$ simplifies to [50]

$$i\hbar\frac{d}{dt}\mathcal{G}_{npjm}^{\uparrow(\downarrow)}(t) - [h_{\uparrow(\downarrow)}^{(2)\mathrm{HF}}, \mathcal{G}^{\uparrow(\downarrow)}]_{npjm}(t) = (i\hbar)^2\sum_{k}U(t)$$
$$\times[G_{nk}^{\uparrow(\downarrow)>}(t,t)G_{pk}^{\downarrow(\uparrow)>}(t,t)G_{kj}^{\uparrow(\downarrow)<}(t,t)G_{km}^{\downarrow(\uparrow)<}(t,t) - > \leftrightarrow <].$$

The numerical effort to solve this equation scales as $\mathcal{O}(N_b^5 N_t^1)$, whereas the original HF-GKBA solution scales as $\mathcal{O}(N_b^3 N_t^2)$, cf. Table I. It turns out that, for the Hubbard model, the new scheme exhibits the most unfavorable scaling with N_b, as compared to the standard scheme and will become advantageous only for sufficiently large N_t. For this reason we choose this case for numerical tests. In Fig. 1 we study the dynamics of a small Hubbard cluster and find excellent agreement between both schemes for all observables, which is demonstrated for the density on site one in Figs. 1(a) and 1(b). An even more sensitive accuracy

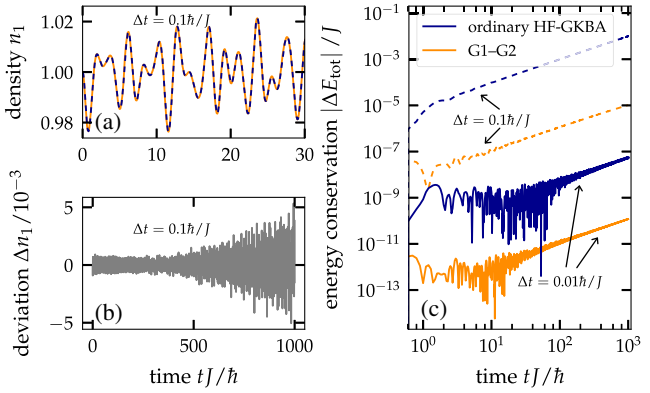

FIG. 1. Comparison of the numerical accuracy of the ordinary HF-GKBA and the G1–G2 scheme with SOA selfenergies, for a four-site Hubbard chain with $U/J = 1.5$, excited by a rapid potential change of amplitude $w_0 = 0.1J$ at site one. (a) Density evolution at the first lattice site, $n_1(t)$. (b) Density difference between both methods, $\Delta n_1(t) = n_1^{\mathrm{G1-G2}}(t) - n_1^{\mathrm{ordinary}}(t)$. (c) Deviation from total-energy conservation for two time steps. Both NEGF implementations are based on a fourth-order integration scheme with the same time step with the initial state being prepared via adiabatic switching [22,31].

test is the conservation of total energy. Here, the G1–G2 scheme turns out to be even more accurate than the standard HF-GKBA scheme if both use the same time step Δt, cf. Fig. 1(c). We now compare in Fig. 2 the CPU time required by both schemes for Hubbard systems with $N_b = 2$ and $N_b = 10$. Our results clearly confirm the quadratic (linear) scaling with N_t of the original HF-GKBA (G1–G2) scheme as well as the predicted scaling with N_b: when going from $N_b = 2$ to $N_b = 10$, "break even" is achieved for N_t approximately $(10/2)^2 = 25$ times larger, for SOA selfenergies.

The uniform electron gas [(UEG), jellium] is a key model for many-body physics, plasma, and condensed-matter physics allowing one to describe important features

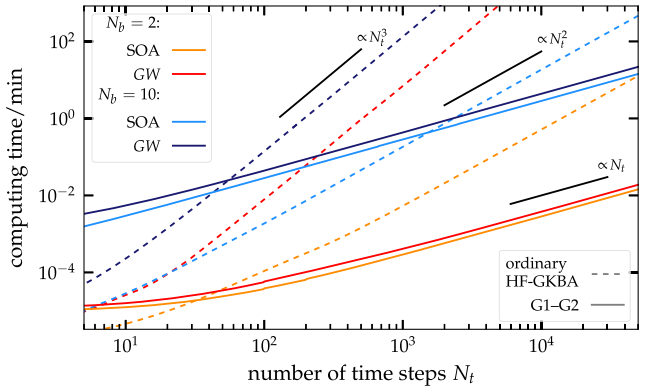

FIG. 2. Log-log comparison of the computational effort of the ordinary HF-GKBA (dashes) and the G1–G2 scheme (full lines) for Hubbard clusters as a function of propagation time N_t. Colors denote system size and the selfenergy approximation.

of the laser-driven nonequilibrium dynamics of electrons in metals [51], warm dense matter [4], and quantum plasmas [2,29], as well as of electron-hole plasmas in semiconductors; see, e.g., Refs. [25,52–54]. Because of homogeneity, a momentum (plain-wave) basis is advantageous where the Green function becomes diagonal: $G_{\boldsymbol{pq}}(t,t') := \delta_{\boldsymbol{pq}} G_{\boldsymbol{p}}(t,t')$, for momenta $\boldsymbol{p}, \boldsymbol{q}$. The Hamiltonian of the UEG in second quantization reads [3]

$$\hat{H}(t) = \sum_{\boldsymbol{p}\alpha} \frac{\boldsymbol{p}^2}{2m} \hat{c}^\dagger_{\boldsymbol{p}\alpha} \hat{c}_{\boldsymbol{p}\alpha} + \sum_{\boldsymbol{p}\boldsymbol{p}'\boldsymbol{q}\alpha\beta} v_{|\boldsymbol{q}|} \hat{c}^\dagger_{\boldsymbol{p}+\boldsymbol{q}\alpha} \hat{c}^\dagger_{\boldsymbol{p}'-\boldsymbol{q}\beta} \hat{c}_{\boldsymbol{p}'\beta} \hat{c}_{\boldsymbol{p}\alpha},$$

with the Coulomb matrix element $v_{|\boldsymbol{q}|} = (4\pi e^2/|\boldsymbol{q}|^2)$. The integral (4) becomes $I_{\boldsymbol{p},\sigma}(t) = \pm i\hbar \sum_{\bar{\boldsymbol{p}},\boldsymbol{q},\alpha} v_{|\boldsymbol{q}|}(t) \mathcal{G}^{\sigma\alpha}_{\boldsymbol{p}\bar{\boldsymbol{p}}\boldsymbol{q}}(t)$, whereas the two-particle Green's function $\mathcal{G}$ obeys

$$\begin{aligned} &i\hbar \frac{d}{dt} \mathcal{G}^{\sigma\alpha}_{\boldsymbol{p}\bar{\boldsymbol{p}}\boldsymbol{q}}(t) - \mathcal{G}^{\sigma\alpha}_{\boldsymbol{p}\bar{\boldsymbol{p}}\boldsymbol{q}}(t)(h^{\mathrm{HF}}_{\boldsymbol{p}-\boldsymbol{q},\sigma} + h^{\mathrm{HF}}_{\bar{\boldsymbol{p}}+\boldsymbol{q},\alpha} - h^{\mathrm{HF}}_{\boldsymbol{p},\sigma} - h^{\mathrm{HF}}_{\bar{\boldsymbol{p}},\alpha}) \\ &= (i\hbar)^2 \{ v_{|\boldsymbol{q}|}(t) \pm \delta_{\sigma,\alpha} v_{|\boldsymbol{p}-\boldsymbol{q}-\bar{\boldsymbol{p}}|}(t) \} \\ &\quad \times [G^{>}_{\boldsymbol{p}-\boldsymbol{q},\sigma}(t,t) G^{>}_{\bar{\boldsymbol{p}}+\boldsymbol{q},\alpha}(t,t) G^{<}_{\boldsymbol{p},\sigma}(t,t) G^{<}_{\bar{\boldsymbol{p}},\alpha}(t,t) - (> \leftrightarrow <)]. \end{aligned} \tag{12}$$

Interestingly, Eq. (12) scales as $\mathcal{O}(N_b^3 N_t^1)$ vs $\mathcal{O}(N_b^3 N_t^2)$, for the standard HF-GKBA, cf. Table I, and the G1–G2 scheme brings about a dramatic acceleration, independent of basis size.

Spectra and two-particle observables.—In addition to accelerating the time evolution, the G1–G2 scheme gives also access to more accurate spectral information. While within the HF-GKBA spectral functions are treated on the Hartree-Fock level, correlation effects in energy spectra can be recovered by investigating the temporal response of the system to a short weak external excitation (linear response), see, e.g., Refs. [35–37]. This is demonstrated in Fig. 3 where the energy spectrum is retrieved via Fourier transform of the density evolution in a Hubbard system. Here the long propagation time enabled by the G1–G2 scheme allows us to resolve correlation effects in the spectra, in particular broadening and shift of peaks as well as the emergence of new states at high energies.

Furthermore, the G1–G2 scheme allows one to compute several quantities that are difficult or even impossible to access within standard NEGF schemes. This includes the nonequilibrium pair-distribution function (PDF) $g(\boldsymbol{r}_1, \sigma_1; \boldsymbol{r}_2, \sigma_2; t)$ and its Fourier transform—the static structure factor. Moreover, dynamic quantities, such as the density- and spin-correlation functions or velocity-autocorrelation functions and the related transport coefficients—the dynamic structure factor, diffusion and absorption coefficients, and the dynamical conductivity within and beyond linear response—are becoming directly accessible. In Fig. 4, we show, as an example, the time evolution of the pair-correlation function (PCF, i.e., the correlated part or the PDF) relative to site 1, $\delta g_{i\uparrow,1\downarrow} = g_{i\uparrow,1\downarrow} - n_{i\uparrow} n_{1\downarrow}$, for a 20-site Hubbard system after an interaction quench, $U/J = 0 \to 2$. Initially the system is ideal, corresponding to $\delta g \equiv 0$, and correlations emerge rapidly and spread with constant speed throughout the system. Changing U does not affect this speed, but the amplitude of the distance-dependent oscillations is proportional to U.

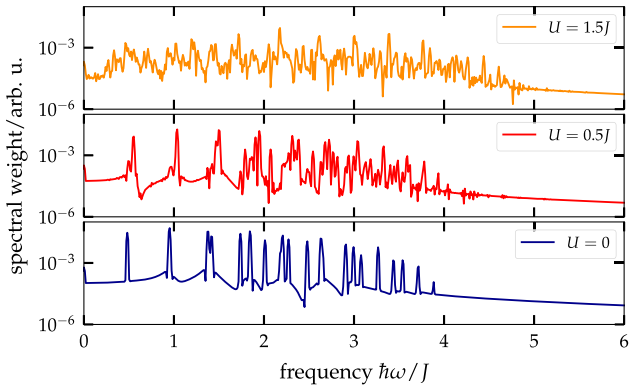

FIG. 3. Excitation spectrum of a 12-site Hubbard chain for three coupling strengths U due to a rapid potential change of amplitude $w_0 = 0.01J$ at site one. The spectrum is obtained via Fourier transform of the density $n_1(t)$ computed with the G1–G2 scheme up to $T = 600\hbar/J$. The initial state is prepared using adiabatic switching.

Extension to advanced selfenergies.—Finally, we test the G1–G2 scheme for the HF-GKBA with *GW* selfenergies which are known to be significantly more accurate than SOA, in particular, at stronger coupling [38,44]. At the same time existing *GW* simulations out of equilibrium scale as N_t^3. Remarkably, we observe that the present G1–G2 scheme achieves order N_t^1 scaling, as is summarized for

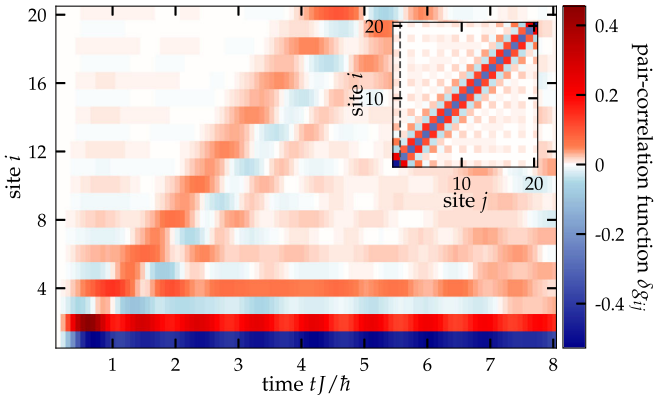

FIG. 4. Time evolution of the PCF relative to site 1, $\delta g_{i\uparrow,1\downarrow}(t)$, for a spatially homogeneous spin-symmetric 20-site Hubbard chain following an interaction quench $U/J = 0 \to 2$ at $t = 0$. Sign-alternating correlations emerge rapidly and approach the correlated ground state (GS). Inset shows $\delta g^{\mathrm{GS}}_{i\uparrow,j\downarrow}$, for $U/J = 2$, computed via adiabatic switching. The dashed line corresponds to data in the main figure.

different basis sets in Table I (details are given in Ref. [41], and similar results are observed for T-matrix selfenergies). The huge computational advantage brought about by G1–G2-GW simulations becomes evident also in Fig. 2; even for Hubbard systems the G1–G2 scheme is advantageous, except for very short simulations. This indicates that a large class of problems is now becoming accessible for accurate NEGF simulations that had remained out of reach so far.

Summary and discussion.—We have implemented an alternative approach to NEGF simulations within the HF-GKBA that is memory-free and achieves the ultimate limit of linear scaling with the propagation duration T, as opposed to the common HF-GKBA approach with SOA (GW) selfenergies that is of order T^2 (T^3). This is achieved by solving coupled time-local equations for $G(t,t)$ and the time-diagonal two-particle Green function $\mathcal{G}(t)$. With this G1–G2 scheme we also established a direct link to the independent reduced-density-matrix (RDM) approach that has become popular in recent years in many fields, see, e.g., Refs. [42,55–60]. Applying our derivation allows one to identify those RDM approximations that are equivalent to common selfenergies in NEGF theory what enables one to make use of the full power of Feynman diagrams in RDM theory. We expect that the demonstrated astonishing scaling of the G1–G2 scheme will make highly accurate NEGF simulations of many nonequilibrium processes such as in laser-excited correlated systems achievable.

We thank K. Balzer for valuable comments. This work was supported by Grant No. shp00015 for CPU time at the Norddeutscher Verbund für Hoch- und Höchstleistungsrechnen (HLRN).

[1] W. Ebeling, V. Fortov, and V. Filinov, *Quantum Statistics of Dense Gases and Nonideal Plasmas*, Springer Series in Plasma Science and Technology (Springer International Publishing, Cham, 2017).

[2] D. Kremp, M. Schlanges, and W. Kraeft, *Quantum Statistics of Nonideal Plasmas* (Springer, Berlin, Heidelberg, 2005).

[3] T. Dornheim, S. Groth, and M. Bonitz, The uniform electron gas at warm dense matter conditions, Phys. Rep. **744**, 1 (2018).

[4] P. Ndione, S. Weber, B. Rethfeld, and D. Gericke, Density response to short-pulse excitation in gold, Contrib. Plasma Phys. **59**, e201800186 (2019).

[5] S. A. Jensen, R. Ulbricht, A. Narita, X. Feng, K. Müllen, T. Hertel, D. Turchinovich, and M. Bonn, Ultrafast photoconductivity of graphene nanoribbons and carbon nanotubes, Nano Lett. **13**, 5925 (2013).

[6] J.-P. Joost, N. Schlünzen, and M. Bonitz, Femtosecond electron dynamics in graphene nanoribbons a nonequilibrium Green functions approach within an extended Hubbard model, Phys. Status Solidi B **256**, 1800498 (2019).

[7] U. Schneider, L. Hackermüller, J. P. Ronzheimer, S. Will, S. Braun, T. Best, I. Bloch, E. Demler, S. Mandt, D. Rasch, and A. Rosch, Fermionic transport and out-of-equilibrium dynamics in a homogeneous Hubbard model with ultracold atoms, Nat. Phys. **8**, 213 (2012).

[8] N. Schlünzen, S. Hermanns, M. Bonitz, and C. Verdozzi, Dynamics of strongly correlated fermions: *Ab initio* results for two and three dimensions, Phys. Rev. B **93**, 035107 (2016).

[9] C. F. de Morisson Faria and X. Liu, Electron–electron correlation in strong laser fields, J. Mod. Opt. **58**, 1076 (2011).

[10] F. Covito, E. Perfetto, A. Rubio, and G. Stefanucci, Benchmarking nonequilibrium Green's functions against configuration interaction for time-dependent Auger decay processes, Eur. Phys. J. B **91**, 216 (2018).

[11] K. Balzer, N. Schlünzen, and M. Bonitz, Stopping dynamics of ions passing through correlated honeycomb clusters, Phys. Rev. B **94**, 245118 (2016).

[12] K. Balzer, M. R. Rasmussen, N. Schlünzen, J.-P. Joost, and M. Bonitz, Doublon Formation by Ions Impacting a Strongly Correlated Finite Lattice System, Phys. Rev. Lett. **121**, 267602 (2018).

[13] E. Perfetto, A.-M. Uimonen, R. van Leeuwen, and G. Stefanucci, First-principles nonequilibrium Green's-function approach to transient photoabsorption: Application to atoms, Phys. Rev. A **92**, 033419 (2015).

[14] K. Balzer, S. Bauch, and M. Bonitz, Time-dependent second-order Born calculations for model atoms and molecules in strong laser fields, Phys. Rev. A **82**, 033427 (2010).

[15] N. Schlünzen, J.-P. Joost, F. Heidrich-Meisner, and M. Bonitz, Nonequilibrium dynamics in the one-dimensional Fermi-Hubbard model: Comparison of the nonequilibrium Green-functions approach and the density matrix renormalization group method, Phys. Rev. B **95**, 165139 (2017).

[16] P. Lipavský, V. Špička, and B. Velický, Generalized Kadanoff-Baym ansatz for deriving quantum transport equations, Phys. Rev. B **34**, 6933 (1986).

[17] A. Kalvova, B. Velicky, and V. Spicka, Beyond the generalized Kadanoff-Baym ansatz, Phys. Status Solidi B **256**, 1800594 (2019).

[18] S. Hermanns, K. Balzer, and M. Bonitz, Few-particle quantum dynamics—Comparing nonequilibrium Green functions with the generalized Kadanoff-Baym ansatz to density operator theory, J. Phys. Conf. Ser. **427**, 012008 (2013).

[19] K. Balzer and M. Bonitz, *Nonequilibrium Green's Functions Approach to Inhomogeneous Systems* (Springer, Berlin, Heidelberg, 2013).

[20] D. Karlsson, R. van Leeuwen, E. Perfetto, and G. Stefanucci, The generalized Kadanoff-Baym ansatz with initial correlations, Phys. Rev. B **98**, 115148 (2018).

[21] M. Bonitz, K. Balzer, N. Schlünzen, M. R. Rasmussen, and J.-P. Joost, Ion impact induced ultrafast electron dynamics in finite graphene-type Hubbard clusters, Phys. Status Solidi B **256**, 1800490 (2019).

[22] S. Hermanns, N. Schlünzen, and M. Bonitz, Hubbard nanoclusters far from equilibrium, Phys. Rev. B **90**, 125111 (2014).

[23] L. Bányai, Q. T. Vu, B. Mieck, and H. Haug, Ultrafast Quantum Kinetics of Time-Dependent RPA-Screened Coulomb Scattering, Phys. Rev. Lett. **81**, 882 (1998).

[24] M. Lorke, T. R. Nielsen, J. Seebeck, P. Gartner, and F. Jahnke, Quantum kinetic effects in the optical absorption of

semiconductor quantum-dot systems, J. Phys. Conf. Ser. **35**, 182 (2006).
[25] Y. Murakami, M. Schüler, S. Takayoshi, and P. Werner, Ultrafast nonequilibrium evolution of excitonic modes in semiconductors, arXiv:1907.06799.
[26] R. Tuovinen, D. Golez, M. Schüler, P. Werner, M. Eckstein, and M. A. Sentef, Adiabatic preparation of a correlated symmetry-broken initial state with the generalized Kadanoff–Baym ansatz, Phys. Status Solidi B **256**, 1800469 (2019).
[27] S. Latini, E. Perfetto, A.-M. Uimonen, R. van Leeuwen, and G. Stefanucci, Charge dynamics in molecular junctions: Nonequilibrium Green's function approach made fast, Phys. Rev. B **89**, 075306 (2014).
[28] A. Kalvova, B. Velicky, and V. Spicka, Generalized master equation for a molecular bridge improved by vertex correction to the generalized Kadanoff–Baym ansatz, Europhys. Lett. **121**, 67002 (2018).
[29] D. Kremp, T. Bornath, M. Bonitz, and M. Schlanges, Quantum kinetic theory of plasmas in strong laser fields, Phys. Rev. E **60**, 4725 (1999).
[30] H. Haberland, M. Bonitz, and D. Kremp, Harmonics generation in electron-ion collisions in a short laser pulse, Phys. Rev. E **64**, 026405 (2001).
[31] N. Schlünzen and M. Bonitz, Nonequilibrium Green functions approach to strongly correlated Fermions in lattice systems, Contrib. Plasma Phys. **56**, 5 (2016).
[32] M. Hopjan and C. Verdozzi, Initial correlated states for the generalized Kadanoff–Baym Ansatz without adiabatic switching-on of interactions in closed systems, Eur. Phys. J. Spec. Top. **227**, 1939 (2019).
[33] R. Tuovinen, F. Covito, and M. A. Sentef, Efficient computation of the second-Born self-energy using tensor-contraction operations, J. Chem. Phys. **151**, 174110 (2019).
[34] E. Perfetto and G. Stefanucci, The dissection algorithm for the second-born self-energy, Phys. Status Solidi B **256**, 1800573 (2019).
[35] N.-H. Kwong and M. Bonitz, Real-time Kadanoff-Baym Approach to Plasma Oscillations in a Correlated Electron Gas, Phys. Rev. Lett. **84**, 1768 (2000).
[36] N. E. Dahlen and R. van Leeuwen, Solving the Kadanoff–Baym Equations for Inhomogeneous Systems: Application to Atoms and Molecules, Phys. Rev. Lett. **98**, 153004 (2007).
[37] M. Bonitz, S. Hermanns, and K. Balzer, Dynamics of Hubbard nano-clusters following strong excitation, Contrib. Plasma Phys. **53**, 778 (2013).
[38] G. Stefanucci and R. van Leeuwen, *Nonequilibrium Many-Body Theory of Quantum Systems* (Cambridge University Press, Cambridge, England, 2013).
[39] P. C. Martin and J. Schwinger, Theory of many-particle systems. I, Phys. Rev. **115**, 1342 (1959).
[40] M. Bonitz, S. Hermanns, K. Kobusch, and K. Balzer, Nonequilibrium Green function approach to the pair distribution function of quantum many-body systems out of equilibrium, J. Phys. Conf. Ser. **427**, 012002 (2013).
[41] See Supplemental Material at http://link.aps.org/supplemental/10.1103/PhysRevLett.124.076601 for the definition of the two-particle time-evolution operator $\mathcal{U}^{(2)}$ and the derivation of the G1–G2 formulas in *GW* approximation.
[42] M. Bonitz, *Quantum Kinetic Theory*, Teubner-Texte zur Physik, 2nd ed. (Springer, Cham, 2016).
[43] The scaling reduction $\mathcal{O}(N_b^8) \to \mathcal{O}(N_b^5)$ is achieved by reordering the occurring tensor contractions, cf. Eq. (9), [44].
[44] N. Schlünzen, S. Hermanns, M. Scharnke, and M. Bonitz, Ultrafast dynamics of strongly correlated fermions—Nonequilibrium Green functions and selfenergy approximations, J. Phys. Condens. Matter **32**, 103001 (2020).
[45] For comparison, the numerical effort of the above-mentioned initial-correlations scheme [20,21] scales as $\mathcal{O}(N_b^5 N_{t^*}^2)$, where N_{t^*} denotes the number of time steps after the buildup of correlations. On the other hand, a scaling of the same order as our G1–G2 scheme has been achieved, e.g., in Ref. [13] by invoking the (drastic) Markov approximation to the GKBA equations, whereas the G1–G2 scheme is an identical reformulation of the original HF-GKBA.
[46] J. Hubbard and B. H. Flowers, Electron correlations in narrow energy bands, Proc. R. Soc. A **276**, 238 (1963).
[47] D. Baeriswyl, D. Campbell, J. Carmelo, F. Guinea, and E. Louis, *The Hubbard Model: Its Physics and Mathematical Physics*, Nato Science Series B (Springer, New York, 2013).
[48] T. Esslinger, Fermi-Hubbard physics with atoms in an optical lattice, Annu. Rev. Condens. Matter Phys. **1**, 129 (2010).
[49] L. Tarruell and L. Sanchez-Palencia, Quantum simulation of the Hubbard model with ultracold fermions in optical lattices, C.R. Phys. **19**, 365 (2018).
[50] The matrix $\mathcal{G}_{npjm}$ occurs with two spin combinations $(\uparrow, \downarrow)$ that are defined by the two possible combinations of spins on the right-hand side.
[51] B. Y. Mueller and B. Rethfeld, Relaxation dynamics in laser-excited metals under nonequilibrium conditions, Phys. Rev. B **87**, 035139 (2013).
[52] N. H. Kwong, M. Bonitz, R. Binder, and H. S. Köhler, Semiconductor Kadanoff-Baym equation results for optically excited electronhole plasmas in quantum wells, Phys. Status Solidi B **206**, 197 (1998).
[53] R. Binder, H. S. Köhler, M. Bonitz, and N. Kwong, Memory effects in the momentum orientation relaxation of electron hole plasmas in semiconductors, Phys. Rev. B **55**, 5110 (1997).
[54] H. Haug and A.-P. Jauho, *Quantum Kinetics in Transport and Optics of Semiconductors* (Springer, Berlin, Heidelberg, 2008).
[55] V. M. Axt and A. Stahl, A dynamics-controlled truncation scheme for the hierarchy of density matrices in semiconductor optics, Z. Phys. B **93**, 195 (1994).
[56] H. Nakatsuji and K. Yasuda, Direct Determination of the Quantum-Mechanical Density Matrix Using the Density Equation, Phys. Rev. Lett. **76**, 1039 (1996).
[57] S. Krönke and P. Schmelcher, Born-Bogoliubov-Green-Kirkwood-Yvon hierarchy for ultracold bosonic systems, Phys. Rev. A **98**, 013629 (2018).
[58] A. Akbari, M. J. Hashemi, A. Rubio, R. M. Nieminen, and R. van Leeuwen, Challenges in truncating the hierarchy of time-dependent reduced density matrices equations, Phys. Rev. B **85**, 235121 (2012).
[59] P. Schuck and M. Tohyama, Self-consistent RPA and the time-dependent density matrix approach, Eur. Phys. J. A **52**, 307 (2016).
[60] F. Lackner, I. Březinová, T. Sato, K. L. Ishikawa, and J. Burgdörfer, High-harmonic spectra from time-dependent two-particle reduced-density-matrix theory, Phys. Rev. A **95**, 033414 (2017).